Microfluidics and Nanofluidics (2022) 26:94
https://doi.org/10.1007/s10404-022-02599-z

RESEARCH PAPER

Predicting actuated contact line pinning forces and the elimination of hysteresis under AC electrowetting

Kimberly A. Bernetski[1] · Hee Tae An[1] · Kara L. Maki[2] · Michael J. Schertzer[1]

Received: 20 May 2022 / Accepted: 8 October 2022 / Published online: 22 October 2022

Abstract

An accurate description of contact angle hysteresis in AC electrowetting is important for a wide range of practical electrowetting applications. This work demonstrates that electrowetting actuated advancing contact angles and the reduction of contact angle hysteresis in AC electrowetting are better predicted when characterizing the advancing electrowetting force by its root mean square (rms) value as opposed to its time-averaged or maximum values. Characterizing the electrowetting force by its rms value allows the transient electrowetting force to exceed the pinning force for some amount of time overcoming the inertial effects at the contact line before advancement. This is opposed to the maximum force characterization which implies that inertial effects can be neglected at the contact line resulting in immediate advancement when the forces are unbalanced.

Keywords Digital microfluidics · Electrowetting on dielectric · Contact angle hysteresis · Contact line pinning

Abbreviations

a	Subscript denoting a property when the contact line is advancing
avg	The time-averaged value of a transient variable. Superscript/subscript denoting the time-averaged value
c	Capacitance per unit area of the solid–liquid interface on an electrowetting on dielectric device
crit	Subscript denoting a property associated with the critical Electrowetting number where contact angle hysteresis is predicted to be eliminated
Ew	Electrowetting number, a ratio of electrical and interfacial energy at the solid–liquid interface and subscript denoting a property under that electrowetting number. Superscript and subscript denoting properties (e.g., contact angle) under electrowetting actuation
f'	Force per unit length at the contact line (in the units of surface tension)
f	Dimensionless force at the contact line
int	Superscript denoting the case where the electrowetting number is such that the cosine of the advancing and receding contact angles both intersect with the electrowetting equation
LM	Subscript denoting a property associated with the interface between the liquid droplet and surrounding medium
max	The maximum value of a transient variable. Superscript/subscript denoting the maximum value
min	The minimum value of a transient variable. Superscript/subscript denoting the minimum value
p	Subscript denoting pinning force
pk	Superscript denoting peak voltage
r	Subscript denoting a property when the contact line is receding
rms	Subscript denoting the root mean square average of a transient variable
SL	Subscript denoting a property associated with the interface between the solid and the liquid droplet

✉ Michael J. Schertzer
mjseme@rit.edu

Kimberly A. Bernetski
kab3322@rit.edu

Hee Tae An
hxa6018@g.rit.edu

Kara L. Maki
kmaki@rit.edu

[1] Mechanical Engineering, Rochester Institute of Technology, 76 Lomb Memorial Drive, Rochester, NY 14623, USA

[2] School of Mathematical Sciences, Rochester Institute of Technology, 85 Lomb Memorial Drive, Rochester, NY 14623, USA

SM	Subscript denoting a property associated with the interface between the solid and the surrounding medium
t	Time
U	Voltage
Y	Superscript denoting the equilibrium contact angle suggested by Young's equation
α	Constant found to scale dimensionless pinning force to electrowetting number for pinning forces under various contact line pinning models
γ	Surface tension between any two phases in the system
θ	Contact angle
ω	Actuation frequency of an electrical voltage
0	Subscript denoting the unactuated condition (i.e., $Ew = 0$)

1 Introduction

Digital microfluidic (DMF) devices use electrowetting on dielectric (EWOD) manipulation of interface shapes and contact line positions of droplets (Cho et al. 2003; Choi et al. 2012; Eral et al. 2011; Mampallil et al. 2012; Mugele and Baret 2005; Nelson and Kim 2012; Orejon et al. 2013; Paik et al. 2003; Samiei et al. 2016). These devices consist of pico- to nanoliter droplets separated from an addressable electrode by one or more polymer films that act as dielectric and hydrophobic layers. The droplets can be confined between two plates (Liu et al. 2021) or unconfined (Burkhart et al. 2020).

When a voltage is applied to the addressable electrode of a DMF device, the apparent contact angle between the droplet and the dielectric is reduced for the portion of the contact line above the electrode. For low to moderate voltages, this behavior is described by the electrowetting (EW) equation:

$$\cos\left(\theta^{Ew}\right) = \cos\left(\theta_Y^0\right) + \frac{cU_{\text{rms}}^2}{2\gamma_{\text{LM}}} = \cos(\theta_Y^0) + Ew. \tag{1}$$

Here, c is the capacitance per unit area of the solid–liquid interface, U_{rms} is the root-mean-squared (rms) voltage, γ_{LM} is the surface tension between the liquid and the surrounding medium, θ_Y^0 is the initial unactuated contact angle, and θ^{Ew} is the apparent contact angle observed at a given rms voltage. The change in the interface shape depends on the electrowetting number (Ew), a ratio of electrical and interfacial energies at the solid–liquid interface (Nelson and Kim 2012). Electrowetting always reduces the apparent contact angle (θ^{Ew}) since Ew is always a positive number.

Electrowetting behavior is well predicted by (1) at low to moderate voltages, but the prediction breaks down above a system-dependent voltage where the contact angle becomes saturated (Klarman et al. 2011; Mugele 2009; Nelson and Kim 2012; Walker and Shapiro 2006). Several potential mechanisms for this phenomenon have been proposed, including: the presence of a divergent electric field near the contact line (Mugele and Heikenfeld 2018; Teng et al. 2020), charge trapping in the dielectric layer (Quinn et al. 2005; Reid et al. 2020), ionization of the medium surrounding the droplet at high voltages (Pollack and Fair 2000), microdroplet ejection (Vallet et al. 1999), and physical deformation that enhances pinning of the contact line on thin, soft dielectric materials (Markodimitrakis et al. 2021).

Comprehensive reviews of DMF devices and their applications have been provided by Mugele and Baret (2005), Nelson and Kim (2012), Choi et al. (2012), and Wang et al. (2017). Commercial activity of DMF devices based on EWOD technology has increased recently (Li and Kim 2020), particularly for liquid lens (e.g., Chen et al. 2021) and lab on a chip (e.g., Coelho et al. 2022) applications.

Contact line mobility between the droplet and the surface is characterized by the advancing and receding contact angles for a given system. The difference between these angles is contact angle hysteresis. The advancing and receding contact angles are defined to be the contact angles at which the contact line pinning force is overcome and the contact line moves either in the advancing or receding directions, respectively. Therefore, a fundamental understanding of contact line pinning in EWOD devices is needed to characterize contact line mobility.

Li and Mugele (2008) predicted electrowetting (EW) actuated advancing and receding contact angles under AC EW by balancing surface tension forces (measured in units of the surface tension), pinning forces, and the EW force at the contact line. Actuated advancing and receding contact angles were predicted using the maximum and minimum values of the EW force, respectively. In Bernetski et al. (2019), we used the same dataset to demonstrate that EW actuated advancing contact angles were predicted more accurately when characterizing the advancing EW force by its rms value. That work also suggested that actuated receding (θ_r^{Ew}) and advancing (θ_a^{Ew}) contact angles should be bounded by the EW Eq. (1). While our model provided more accurate predictions of previously published experimental data, Li and Mugele (2008, 2019) argued that (i) there was no physical justification for characterizing the EW force by its rms value and (ii) taking the rms value is incorrect as the rms response of the droplet is already accounted for through the use of the rms voltage in the electrowetting number.

This work tests the hypothesis that predictions for EW actuated advancing contact angles and contact angle hysteresis are improved when the EW force is characterized by its rms value. Experimental data will be compared to model predictions on EWOD devices coated with a variety of polymer films.

2 Mathematical model

As originally shown by Li and Mugele (2008), contact line pinning forces for AC EWOD can be derived by examining the contact line and balancing the dimensional electrowetting force (f'_{Ew}) with surface tensions between the solid and the liquid droplet (γ_{SL}), the solid and the surrounding medium (γ_{SM}), and the liquid and the surrounding medium (γ_{LM}) (Fig. 1a). For an arbitrary actuated contact angle (θ^{Ew}), the dimensional actuated pinning force (f'^{Ew}_p), measured in units of γ_{LM}, is given by

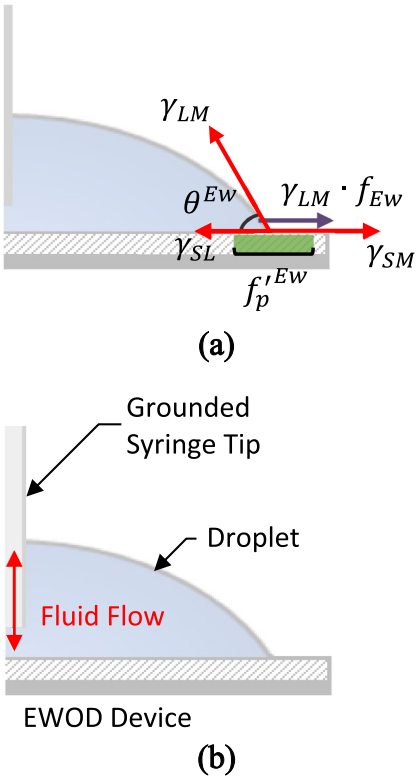

Fig. 1 Sketches of the axisymmetric droplet showing **a** forces per unit length acting on the contact line under AC electrowetting. These forces include all three components of surface tension ($\gamma_{SL}, \gamma_{LM}, \gamma_{SM}$, red), the electrostatic force due to electrowetting ($\gamma_{LM} \bullet f_{Ew}$, purple), and the range of potential actuated pinning forces (f'^{Ew}_p, shaded green); and (**b**) the experimental facility used in this investigation

$$f'^{Ew}_p = \gamma_{SL} - \gamma_{SM} + \gamma_{LM}\cos\left(\theta^{Ew}\right) - f'_{Ew}. \tag{2}$$

After substituting Young's equation and scaling by γ_{LM}, (2) becomes

$$f^{Ew}_p = \cos\left(\theta^{Ew}\right) - \cos\left(\theta^0_Y\right) - f_{Ew}, \tag{3}$$

where θ^0_Y is the unactuated equilibrium contact angle, and f^{Ew}_p and f_{Ew} are the dimensionless actuated pinning and electrowetting forces, respectively. Note that the electrowetting Eq. (1) is found by setting f^{Ew}_p to zero and f_{Ew} to Ew in Eq. (3).

Expressions for advancing and receding pinning forces under AC EW can be determined by replacing the arbitrary actuated contact angle (θ^{Ew}) with actuated advancing (θ^{Ew}_a) or receding (θ^{Ew}_r) contact angles:

$$f^{Ew}_{p,r} = \cos\left(\theta^{Ew}_r\right) - \cos\left(\theta^0_Y\right) - f^r_{Ew}, \tag{4a}$$

$$f^{Ew}_{p,a} = \cos\left(\theta^{Ew}_a\right) - \cos\left(\theta^0_Y\right) - f^a_{Ew}. \tag{4b}$$

Analytical expressions for the cosines of the actuated advancing and receding contact angles can then be constructed by assuming that the dimensionless advancing and receding pinning forces are independent of electrowetting number (Li and Mugele 2008) (that is, $f^{Ew}_{p,r} = f^0_{p,r} = \cos\left(\theta^0_r\right) - \cos(\theta^0_Y)$ and $f^{Ew}_{p,a} = f^0_{p,a} = \cos\left(\theta^0_a\right) - \cos(\theta^0_Y)$) such that

$$\cos\left(\theta^{Ew}_r\right) = \cos\left(\theta^0_r\right) + f^r_{Ew}, \tag{5a}$$

$$\cos\left(\theta^{Ew}_a\right) = \cos\left(\theta^0_a\right) + f^a_{Ew}. \tag{5b}$$

Predicting AC actuated contact angle hysteresis using (5a, 5b) requires the definition of characteristic AC EW forces in the advancing and receding directions. The transient dimensionless AC EW force for sinusoidal waveforms is given by

$$\begin{aligned} f_{Ew}(t) &= \frac{cU^2_{pk}}{2\gamma_{LM}}\sin^2(\omega t) = 2\frac{cU^2_{rms}}{2\gamma_{LM}}\sin^2(\omega t) \\ &= 2Ew\sin^2(\omega t) = Ew[1-\cos(2\omega t)], \end{aligned} \tag{6}$$

where again, c is the capacitance per unit area of the device, U_{pk} is the peak voltage, U_{rms} is the rms voltage, ω is the actuation frequency, and Ew is the electrowetting number. It is important to note that use of U_{rms} and Ew (which is a function of U_{rms}) in (6) is a mathematical simplification ($U_{pk} = \sqrt{2}U_{rms}$) and not the result of computing a root mean square (rms) average of the transient electrowetting force.

Li and Mugele proposed that the EW force in the receding and advancing cases should be characterized by the minimum

$$f_{Ew}^{r} = f_{Ew}^{min} = \min\left(f_{Ew}(t)\right) = 0, \tag{7}$$

and maximum

$$f_{Ew}^{a} = f_{Ew}^{\max} = \max\left(f_{Ew}(t)\right) = 2Ew \tag{8}$$

values, respectively (Li and Mugele 2008). This characterization assumes that the liquid responds almost instantaneously to $f_{Ew}(t)$ because the appropriate length scale at the contact line is the characteristic size of surface inhomogeneities, not the droplet size (Li and Mugele 2008, 2019). Predictions for actuated advancing and receding contact angles under EW can be attained by substituting (7) and (8) into (5a) and (5b), respectively. Predicted receding contact angles (θ_r^{Ew}) agreed well with experimental data prior to the intersection of the model with the EW Eq. (1) (Bernetski et al. 2019; Li and Mugele 2008), where the unactuated equilibrium contact angle is $\theta_0^Y \approx \left(\cos\theta_r^0 + \cos\theta_a^0\right)/2$. As shown by Bernetski et al. (2019), the maximum electrowetting force may not provide the most accurate characterization for the advancing case.

The rms value of the transient electrowetting force is given by

$$f_{Ew}^{a} = f_{Ew}^{\text{rms}} = \text{rms}\left(f_{Ew}(t)\right) = \left(\frac{1}{\omega/\pi}\int_0^{\omega/\pi}\left[f_{Ew}(t)\right]^2 dt\right)^{1/2} = \sqrt{3/2}Ew, \tag{9}$$

where the bounds of integration are set to one period for $\sin^2(\omega t)$. This characterization suggests that inertial and viscous forces at the contact line prevent instantaneous motion when the forces at the contact line are unbalanced (Li and Mugele 2019). A future study, in which fluid properties are varied, could be used to test this proposed mechanism.

For completeness, the time-averaged value of the electrowetting force is also considered and is given by

$$f_{Ew}^{a} = f_{Ew}^{avg} = \overline{f_{Ew}(t)} = \frac{1}{\omega/\pi}\int_0^{\omega/\pi} f_{Ew}(t)\mathrm{d}t = Ew. \tag{10}$$

This characterization suggests that damping at the contact line is large enough that contact line motion is governed by the time-averaged EW force. It also suggests that contact line dynamics in the AC actuated case would be the same as those of the DC case; this is contradictory to observations of transient contact line oscillation under AC EW, such as those presented by Mannetje et al. (2013).

The selection of a characteristic advancing EW force changes the prediction of the dependence of actuated advancing contact angles on the electrowetting number. The characteristic advancing EW force can be cast as

$$f_{Ew}^{a} = \alpha Ew, \tag{11}$$

where $\alpha = 1$ for the time-averaged characterization (10), $\alpha = \sqrt{3/2}$ for the rms value (9), and $\alpha = 2$ for the maximum characterization (8). Actuated receding and advancing contact angles can be predicted by substituting either (7) or (11) into (5a) or (5b) such that

$$\cos\left(\theta_r^{Ew}\right) = \begin{cases} \cos\left(\theta_r^0\right) + 0, Ew < Ew_r^{\text{int}}, \\ \left(\cos\theta_r^0 + \cos\theta_a^0\right)/2 + Ew, Ew \geq Ew_r^{\text{int}}, \end{cases} \tag{12a}$$

$$\cos\left(\theta_a^{Ew}\right) = \begin{cases} \cos(\theta_a^0) + \alpha Ew, Ew < Ew_a^{\text{int}}, \\ \left(\cos\theta_r^0 + \cos\theta_a^0\right)/2 + Ew, Ew \geq Ew_a^{\text{int}}, \end{cases} \tag{12b}$$

where

$$Ew_r^{\text{int}} = \Delta\cos(\theta^0)/2. \text{ and } Ew_a^{\text{int}} = \Delta\cos(\theta^0)/2(\propto -1), \tag{12c}$$

represent the electrowetting numbers at which the predicted advancing and receding contact angles intersect with the EW Eq. (1) and $\Delta\cos(\theta^0) = \cos\theta_r^0 - \cos\theta_a^0$. Piecewise functions (12a) and (12b) are required as $\cos(\theta_a^{Ew})$, $\cos(\theta_r^{Ew})$, and $\cos(\theta^{Ew})$ may not all intersect at the same Ew as predicted by Li and Mugele (2008).

The critical electrowetting number (Ew_{crit}) is the lowest Ew at which contact angle hysteresis is eliminated (i.e., $\cos\left(\theta_r^{Ew}\right) = \cos\left(\theta_a^{Ew}\right)$). The value of Ew_{crit} can be predicted analytically by finding the electrowetting number where $\cos\left(\theta_r^{Ew}\right)$ (12a) and $\cos\left(\theta_a^{Ew}\right)$ (12b) both intersect the electrowetting Eq. (1). This occurs when

$$Ew_{\text{crit}} = \max\left(Ew_r^{\text{int}}, Ew_a^{\text{int}}\right) = \Delta\cos(\theta^0)/2(\propto -1). \tag{13}$$

Note that $Ew_{\text{crit}} = \infty$, when $\alpha = 1$, because the predicted actuated advancing contact angle is parallel to the electrowetting equation in this case. We do not expect this characterization to hold in the AC case as Li and Mugele demonstrated a decrease in contact angle hysteresis (i.e., $\alpha > 1$) under AC EW, but not DC EW ($\alpha = 1$) (Li and Mugele 2008).

3 Experimental section

The models presented above were tested using an experimental set up consisting of an EWOD device, a contact angle measurement system, and deionized water droplets (Fig. 1b). Deionized water droplets (3 μ L) were deposited on EWOD devices consisting of a single unpatterned electrode with upper surfaces of either polytetrafluorethylene (PTFE, Teflon AF) $\theta_Y^0 \approx 121°$ or SU-8 3005 $\theta_Y^0 \approx 80°$. Droplets were grounded using the metallic syringe tip ($D = 0.7$mm) of a Ramé–Hart microdispenser. They were actuated using a 1 kHz AC signal that was produced by an NI PXI-5402 signal generator and amplified to 200 V_{rms} using a Trek PZD700A amplifier. An image of the experimental facility

and a representative image showing a droplet and measured contact angles is shown in supplemental figure, Fig. S1.

Both EWOD device configurations were made using glass slides coated with 100 nm of aluminum. Polymer layers of each device type (beginning with layers closest to the substrate) were as follows: (i) on PTFE/Teflon devices, a dielectric layer of SU-8 3005 (6.2 µm) and hydrophobic layer of Teflon AF (100 nm) and (ii) on SU-8 devices, hybrid dielectric/hydrophobic layer of SU-8 3005 (6.2 µm). SU-8 films were deposited using a two-stage spin coating process (500 rpmrpm for 10 s; 4000 rpm for 30 s; acceleration of 300 rpm/s between stages) before being soft baked (Fisher Scientific Isotemp) for two and a half minutes at 95 ℃, cured in an Electro-Lite EC-500 (365 nm for 30 s), and hard baked for 3 min at 150 ℃. Teflon films were spun onto devices at 2000 rpm for one minute and hard baked at 160 ℃ for ten minutes. A schematic of the step-by-step fabrication process for these devices is provided in supplemental figure, Fig. S2.

Contact angles were measured from side view images of droplets captured with a Ramé-Hart 250 Goniometer with DROPimage Advanced software. A Ramé-Hart automated dispensing system was used to add and remove fluid from droplets at constant rate ($0.21 \pm 0.04 \mu L/s$) as in our previous work (Bernetski et al. 2018). Representative experimental images of advancing (Fig. 2a–d) and receding (Fig. 2e–h) contact angles actuated at $120V_{rms}$ ($Ew \approx 0.50$) on a Teflon-coated EWOD device are shown in Fig. 2. Reported contact angles were averaged from the left and right sides of the moving contact line across five trials for each case (Fig. S1b).

All measurements reported here were repeated at least five times and error bars on related figures represent two standard deviations (95% confidence interval).

4 Results and discussion

Electrowetting curves for both device types are presented in Fig. 3. The evolution of θ^{Ew} with Ew is consistent with the electrowetting Eq. (1) prior to the onset of contact angle saturation. Contact angle saturation was observed between $0.35 < Ew < 0.5$ on both Teflon-coated and SU-8 coated devices. These results suggest that the devices used here perform as expected.

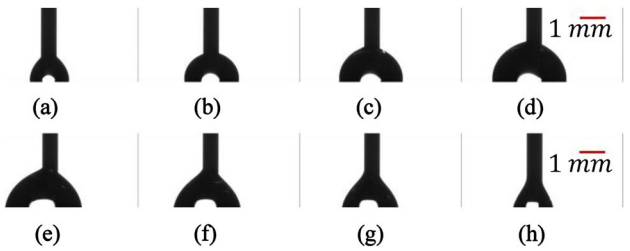

Fig. 2 Experimental images used to calculate **a**–**d** advancing and **e**–**h** receding contact angles for a Teflon-coated EWOD device with an actuation voltage of $120V_{rms}$ ($Ew \approx 0.50$). Grounded syringe tip has a diameter of 0.7mm

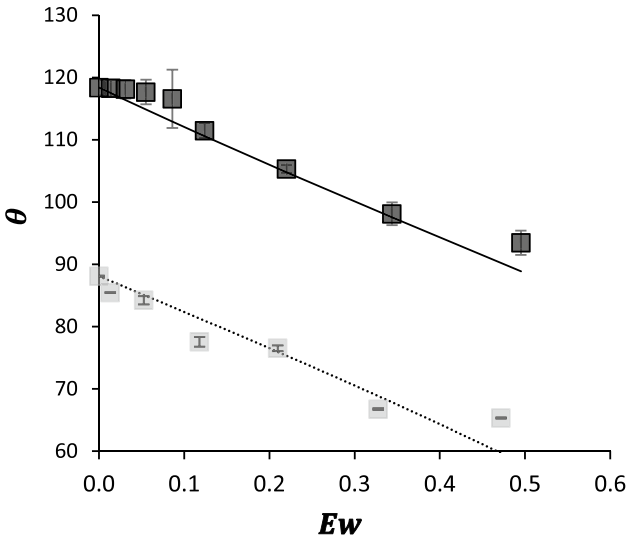

Fig. 3 Experimentally observed actuated apparent contact angles (θ^{Ew}) on devices coated with Teflon (black) and SU-8 (grey) as a function of Ew. Solid (Teflon) and dotted (SU-8) lines show predictions from the EW equation for each device type

As in Bernetski et al. (2019), actuated advancing contact angles on Teflon-coated EWOD devices were predicted more accurately when using the rms value of the EW force

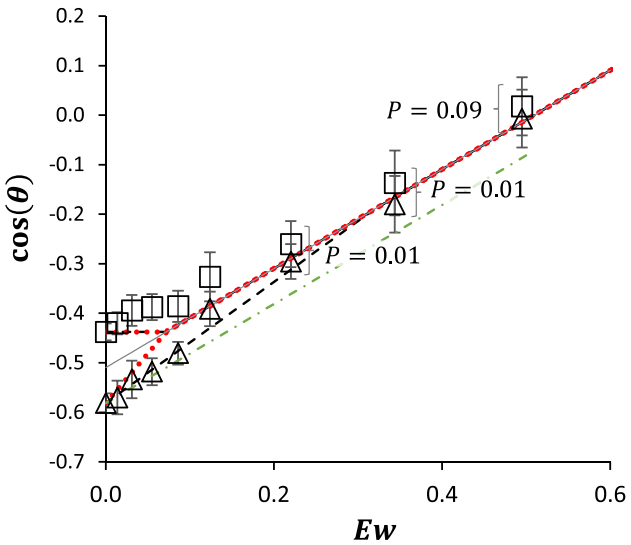

Fig. 4 Cosines of AC actuated advancing (open triangles) and receding (open squares) contact angles on Teflon EWOD devices. Receding (12a) and advancing (12b) contact angle predictions for $\alpha_{max} = 2$ (red dotted), $\alpha_{rms} = \sqrt{3/2}$ (black dash), and $\alpha_{avg} = 1$ (green dot-dash) are shown with the EW equation before (solid gray) and after intersection with the predicted receding angle (12a)

($\alpha_{rms} = \sqrt{3/2}$) instead of the maximum ($\alpha_{max} = 2$), or time-averaged ($\alpha_{avg} = 1$) values (Fig. 4). An experimentally observed value of α was determined using a linear regression of experimental values for $\cos(\theta_a^{Ew})$ prior to the onset of contact angle saturation ($Ew \approx 0.35$). The observed α was 1.20 ± 0.09, where the uncertainty represents the 99.7% confidence interval (Fig. 5a). A similar value for α (1.21 ± 0.16) was found by performing a linear regression on the experimental data shown in Li and Mugele (Li and Mugele 2008) (Fig. 5b). In both of these cases, $\alpha_{rms} = \sqrt{3/2} \approx 1.225$ agrees with the observed value to within 2%. The error in the $\alpha_{max} = 2$ prediction was more than an order of magnitude greater (64%) than the α_{rms} prediction. The maximum prediction was also outside the 99.7% confidence interval of the observed data in both cases. This supports the hypothesis from Bernetski et al. (2019) that the rms value of the EW force is a better choice for the characteristic EW force in the advancing direction.

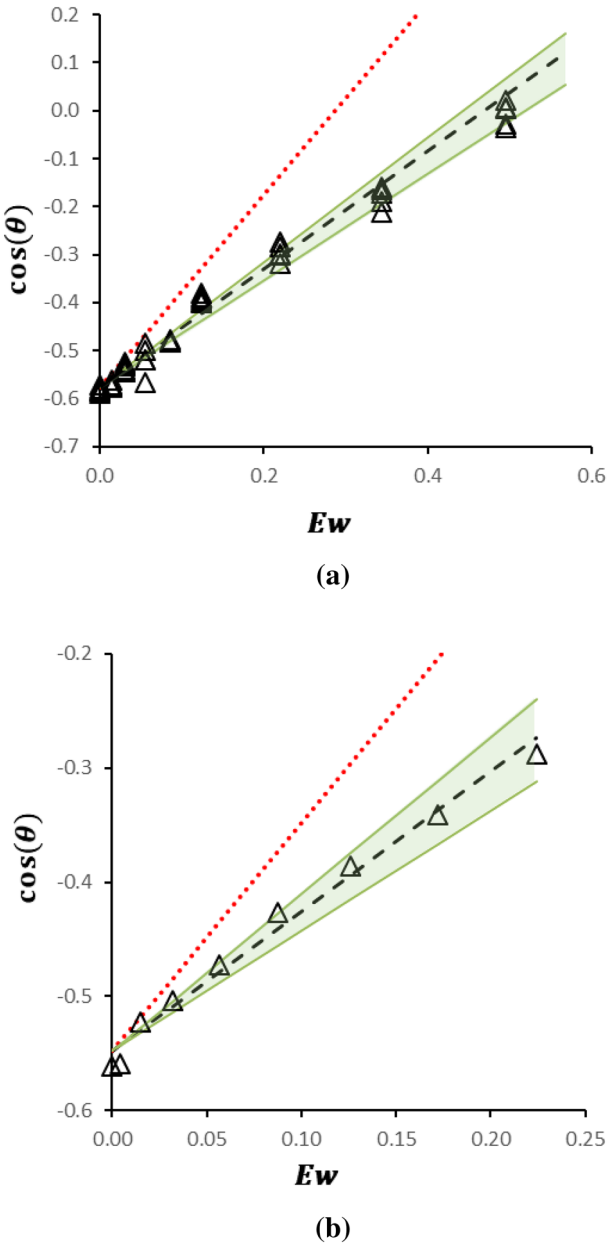

Fig. 5 Cosines of AC actuated advancing (open triangles) contact angles as a function of Ew on Teflon EWOD devices. Advancing angle predictions for $\alpha_{max} = 2$ (red dotted), $\alpha_{rms} = \sqrt{3/2}$ (black dashed) are shown along with the 99.7% confidence interval for the observed value of α (green shaded). Data and predictions for cases from **a** this investigation and **b** Li and Mugele (2008)

Predictions for the advancing and receding actuated contact angles can also be tested by comparing the accuracy of critical Ew predictions from (13). Evaluation of these predictions was not possible in the prior work by Bernetski et al. (2019), because it analyzed the dataset from Li and Mugele (2008) and Ew_{crit}^{rms} was beyond the range of electrowetting numbers explored experimentally.

Critical electrowetting number predictions using the rms EW force ($Ew_{crit}^{rms} = 0.32$) were more accurate than those using the maximum EW force ($Ew_{crit}^{max} = 0.07$) (Fig. 4). Experimentally observed hysteresis was still measurable near Ew_{crit}^{max}, where $\Delta\cos(\theta^{Ew}) = 0.13$ at $Ew = 0.063$ and $\Delta\cos(\theta^{Ew}) = 0.09$ at $Ew = 0.099$. Near Ew_{crit}^{rms} ($Ew = 0.34$), observed contact angle hysteresis was smaller ($\Delta\cos(\theta^{Ew}) \approx 0.035$), but still statistically significant ($P < 0.01$). Observed contact angle hysteresis only became statistically insignificant ($P \approx 0.09$), after the onset of contact angle saturation ($Ew = 0.49$). While it is not clear if hysteresis would have been eliminated if saturation did not occur, the predictions using the rms EW force were again more accurate than those using the maximum EW force.

As on the Teflon surface, predictions for the actuated receding contact angle on SU-8 coated devices are coincident with the previous model (Bernetski et al. 2019; Li and Mugele 2008) and predictions for the actuated advancing contact angle are significantly improved when EW force is characterized by its rms value ($\alpha_{rms} = \sqrt{3/2}$) rather than the maximum ($\alpha_{max} = 2$) (Fig. 6a). On SU-8, the observed value of α calculated prior to the onset of contact angle saturation ($Ew \approx 0.32$) was 1.28 ± 0.11 (Fig. 6b). Again, the error in the α_{rms} prediction (4.2%) is much is smaller than the α_{max} prediction (59%) and the α_{max} prediction falls outside the 99.7% confidence interval from the observed data.

Contact angle hysteresis measurements on the SU-8 coated devices also suggest that α_{rms} provides a more accurate prediction than α_{max}. Hysteresis was still observable ($\Delta\cos\left(\theta^{Ew}\right) \approx 0.13$) at $Ew_{crit}^{max} = 0.15$ (Fig. 6a). While observed hysteresis decreased when Ew was increased above Ew_{crit}^{max} (e.g., $\Delta\cos\left(\theta^{Ew}\right) = 0.10$ at $Ew = 0.21$), contact angle saturation occurred before encountering $Ew_{crit}^{rms} = 0.69$.

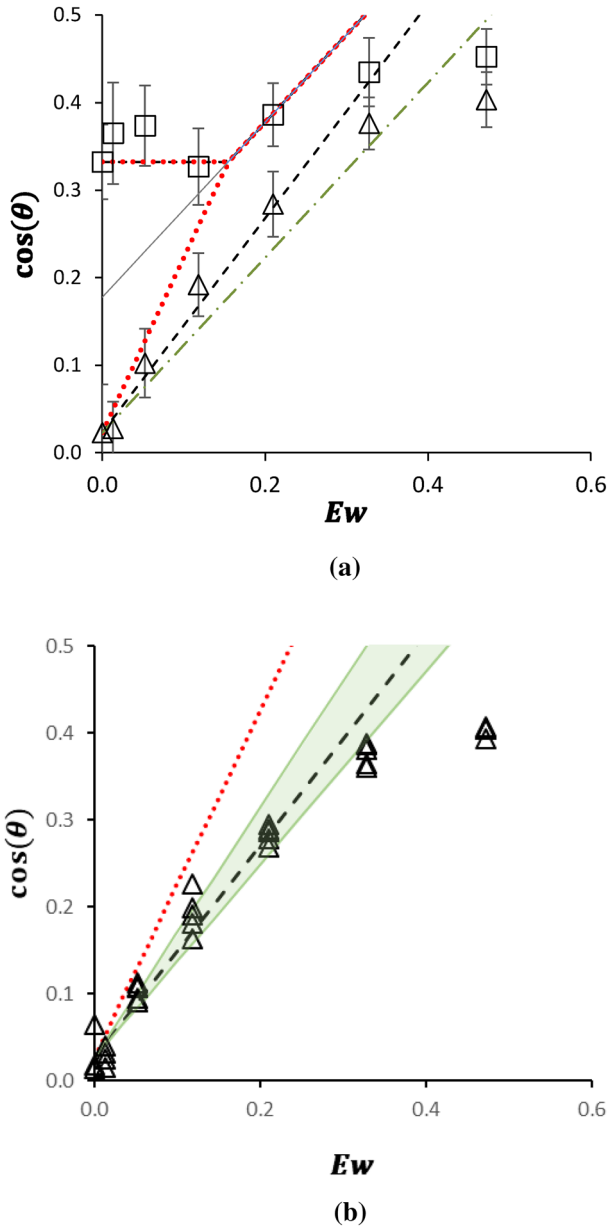

Fig. 6 **a** Cosines of AC actuated advancing (open triangles) and receding (open squares) contact angles on SU-8 EWOD devices. Receding (12a) and advancing (12b) contact angle predictions for $\alpha_{max} = 2$ (red dotted), $\alpha_{rms} = \sqrt{3/2}$ (black dash) and $\alpha_{avg} = 1$ (green dot-dash) are shown along with the EW equation before (solid gray) and after intersection with the predicted receding angle (12a). **b** $\cos\left(\theta_a^{Ew}\right)$ as a function of *Ew* along with the 99.7% confidence interval for the observed value of α (green shaded)

5 Conclusions

This investigation supports the hypothesis that electrowetting actuated advancing contact angles should be characterized using the root mean square (rms) value of the transient electrowetting force and not the maximum value or the time-averaged value. Characterizing the electrowetting force by its rms value suggests that the transient electrowetting force must exceed the pinning force for some amount of time to overcome inertial effects at the contact line before advancement. This is opposed to the maximum force characterization, which implies that inertial effects can be neglected at the contact line resulting in immediate advancement when the forces are unbalanced.

Advancing and receding actuated contact angles were measured experimental over a range of electrowetting numbers on EWOD devices with two different practically relevant hydrophobic coatings. The slope of the cosine of the actuated advancing contact angle with electrowetting number (α) was estimated using linear regression and compared to theoretically predicted values of $\alpha_{rms} = \sqrt{3/2}$, $\alpha_{max} = 2$, and $\alpha_{avg} = 1$.

Observed values of α were calculated from experiments on two surfaces here and one from a previously published study. In all three cases, predictions using α_{rms} agreed with the observed slope to within 2–5% while the error in predictions using α_{max} were over an order of magnitude greater (59% and 64%). Furthermore, the slope from the α_{max} prediction was outside the 99.7% confidence interval for the observed slope in all cases examined here.

The improved actuated advancing contact angle predictions using the rms value of the EW force also led to better predictions of contact angle hysteresis and the critical electrowetting number (Ew_{crit}) at which hysteresis is eliminated. Critical electrowetting number predictions using α_{rms} for were four to five times larger than those using α_{max} for the surfaces examined here. On both surfaces, contact angle hysteresis was large at Ew_{crit} values predicted using α_{max}. On Teflon-coated devices, hysteresis was small but still present at Ew_{crit} values predicted using α_{rms}. On SU-8, hysteresis decreased when *Ew* was increased beyond the value predicted by α_{max}, but contact angle saturation was observed prior to the Ew_{crit} predicted using α_{rms}.

Supplementary Information The online version contains supplementary material available at https://doi.org/10.1007/s10404-022-02599-z.

Acknowledgements We gratefully acknowledge support from ADVANCE RIT (funded through the National Science Foundation under Award No. HRD-1209115) and the Kate Gleason College of Engineering at RIT.

Funding Partial financial support was received from ADVANCE RIT (funded through the National Science Foundation under Award No. HRD-1209115) and the Kate Gleason College of Engineering at RIT.

Data availability statement The datasets generated during and/or analyzed during the current study are available from the corresponding author on reasonable request.

Declarations

Conflict of interest The authors have no relevant financial conflicts of interests to disclose. Dr. Schertzer's research group received funding from an industrial partner to work on a project where the industrial partner was also working with Associate Editor Dr. Hywel Morgan. However, Dr. Schertzer and Dr. Morgan never directly collaborated on interacted on the project.

References

Bernetski KA, Burkhart CT, Maki KL, Schertzer MJ (2018) Characterization of electrowetting, contact angle hysteresis, and adhesion on digital microfluidic devices with inkjet-printed electrodes. Microfluid Nanofluid 22(96):1–10. https://doi.org/10.1007/s10404-018-2119-4

Bernetski KA, Maki KL, Schertzer MJ (2019) Comment on "how to make sticky surfaces slippery: contact angle hysteresis in electrowetting with alternating voltage". Appl Phys Lett 114: 116101–116102. https://doi.org/10.1063/1.5087712

Burkhart CT, Maki KL, Schertzer MJ (2020) Coplanar electrowetting-induced droplet detachment from radially symmetric electrodes. Langmuir 36(28):8129–8136. https://doi.org/10.1021/acs.langmuir.0c01015

Cho SK, Moon H, Kim C-JJ (2003) Creating, transporting, cutting, and merging liquid droplets by electrowetting-based actuation for digital microfluidic circuits. J Microelectromech Syst 12(1):70–80. https://doi.org/10.1109/JMEMS.2002.807467

Choi K, Ng AHC, Fobel R, Wheeler AR (2012) Digital microfluidics. Annu Rev Anal Chem (Palo Alto, Calif.) 5: 413–440. https://doi.org/10.1146/annurev-anchem-062011-143028

Eral HB, Augustine DM, Duits MHG, Mugele F (2011) Suppressing the coffee stain effect: how to control colloidal self-assembly in evaporating drops using electrowetting. Soft Matter 7(10):4954. https://doi.org/10.1039/c1sm05183k

Klarman D, Andelman D, Urbakh M (2011) A model of electrowetting, reversed electrowetting, and contact angle saturation. Langmuir 27(10):6031–6041. https://doi.org/10.1021/la2004326

Li J, Kim CJ (2020) Current commercialization status of electrowetting-on-dielectric (EWOD) digital microfluidics. Lab Chip 20(10):1705–1712. https://doi.org/10.1039/d0lc00144a

Li F, Mugele F (2008) How to make sticky surfaces slippery: contact angle hysteresis in electrowetting with alternating voltage. Appl Phys Lett 92(24):12–15. https://doi.org/10.1063/1.2945803

Li F, Mugele F (2019) Response to "Comment on 'how to make sticky surfaces slippery: contact angle hysteresis in electrowetting with alternating voltage'" Appl Phys Lett 114(11):116101–116102. https://doi.org/10.1063/1.5087712

Liu R, Yang YR, Wang XD (2021) Electrowetting-on-dielectric-induced nanodroplet splitting between two parallel plates. Microfluid Nanofluid 25(1):1–12. https://doi.org/10.1007/s10404-020-02409-4

Mampallil D, Eral HB, van den Ende D, Mugele F (2012) Control of evaporating complex fluids through electrowetting. Soft Matter 8(41):10614. https://doi.org/10.1039/c2sm26103k

Markodimitrakis IE, Sema DG, Chamakos NT, Papadopoulos P, Papathanasiou AG (2021) Impact of substrate elasticity on contact angle saturation in electrowetting. Soft Matter 17(16):4335–4341. https://doi.org/10.1039/d0sm02281k

Mugele F (2009) Fundamental challenges in electrowetting: from equilibrium shapes to contact angle saturation and drop dynamics. Soft Matter 5(18):3377. https://doi.org/10.1039/b904493k

Mugele F, Baret J-C (2005) Electrowetting: from basics to applications. J Phys Condens Matter 17(28):R705–R774. https://doi.org/10.1088/0953-8984/17/28/R01

Mugele F, Heikenfeld J (2018) Electrowetting: fundamental principles and practical applications. Wiley

Nelson WC, Kim C-J (2012) Droplet actuation by electrowetting-on-dielectric (EWOD): a review. J Adhes Sci Technol 26(12–17):1747–1771. https://doi.org/10.1163/156856111X599562

Orejon D, Sefiane K, Shanahan MER (2013) Evaporation of nanofluid droplets with applied DC potential. J Colloid Interface Sci 407:29–38. https://doi.org/10.1016/j.jcis.2013.05.079

Paik P, Pamula VK, Pollack MG, Fair RB (2003) Electrowetting-based droplet mixers for microfluidic systems. Lab Chip 3(1):28–33. https://doi.org/10.1039/b210825a

Pollack MG, Fair RB (2000) Electrowetting-based actuation of liquid droplets for microfluidic applications. Appl Phys Lett 77(11):1725–1726

Quinn A, Sedev R, Ralston J (2005) Contact angle saturation in electrowetting. J Phys Chem B 109(13):6268–6275. https://doi.org/10.1021/jp040478f

Reid RC, Merrill MH, Thomas JP (2020) Stick–slip behavior during electrowetting-on-dielectric: polarization and substrate effects. Microfluid Nanofluid 24(10):1–9. https://doi.org/10.1007/s10404-020-02374-y

Samiei E, Luka GS, Najjaran H, Hoorfar M (2016) Integration of biosensors into digital microfluidics: impact of hydrophilic surface of biosensors on droplet manipulation. Biosens Bioelectron 81:480–486. https://doi.org/10.1016/j.bios.2016.03.035

Teng P, Tian D, Fu H, Wang S (2020) Recent progress of electrowetting for droplet manipulation: from wetting to superwetting systems. Mater Chem Front 4(1):140–154. https://doi.org/10.1039/c9qm00458k

't Mannetje DJCM, Mugele F, van den Ende D (2013) Stick–slip to sliding transition of dynamic contact lines under AC electrowetting. Langmuir 29(48):15116–15121https://doi.org/10.1021/la402761m

Vallet M, Vallade M, Berge B (1999) Limiting phenomena for the spreading of water on polymer films by electrowetting. Eur Phys J B 11(4):583–591. https://doi.org/10.1007/s100510051186

Walker S, Shapiro B (2006) Modeling the fluid dynamics of electrowetting on dielectric (EWOD). J Microelectromech Syst 15(4):986

Wang H, Chen L, Sun L (2017) Digital microfluidics: a promising technique for biochemical applications. Front Mech Eng 12(4):510–525. https://doi.org/10.1007/s11465-017-0460-z